THE JOURNAL OF PHYSICAL CHEMISTRY C

Article

pubs.acs.org/JPCC

Co_3O_4 Nanosheets with In-Plane Pores and Highly Active {112} Exposed Facets for High Performance Lithium Storage

Renjie Wei,[†,‡] Xianlong Zhou,[§] Tengfei Zhou,[§] Juncheng Hu,*[,§] and Johnny C. Ho*[,†,‡]

[†]Department of Materials Science and Engineering, City University of Hong Kong, Kowloon 999077, Hong Kong

[‡]State Key Laboratory of Millimeter Waves, City University of Hong Kong, Kowloon 999077, Hong Kong

[§]Key Laboratory of Catalysis and Materials Science of the State Ethnic Affairs Commission & Ministry of Education, South-Central University for Nationalities, Wuhan 430074, China

Supporting Information

ABSTRACT: Recently, two-dimensional transition metal oxide nanomaterials have been extensively investigated as promising candidates for the lithium-ion battery anode materials due to their elastic volume change, efficient ion/electrical pathways, and additional interfacial lithium storage sites. Herein, we report a simple wet-chemical method followed by thermal treatment to synthesize Co_3O_4 nanosheets with the in-plane pores. The as-prepared nanosheets are found to selectively expose the highly active {112} facets as the dominant surfaces. When fabricated into the anode configuration, a specific capacity of 1717 mA h g^{-1} can be reliably retained after 100 cycles at a current density of 200 mA g^{-1}. While increasing the current density to 1 A g^{-1} and prolonging the cycle life to 400 cycles, the nanosheets can still deliver a capacity of 1090 mA h g^{-1} with a Coulombic efficiency of 99.5%. This excellent electrochemical performance can be attributed to the unique morphological structures of our porous nanosheets for the shortened lithium ion diffusion pathway, alleviated volume expansion, and enhanced active sites, indicating the technological potency of the nanosheets for high-performance lithium storage.

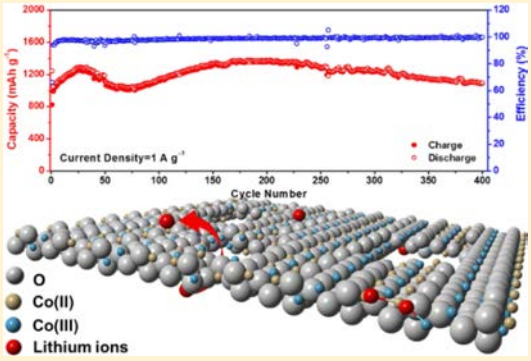

1. INTRODUCTION

In recent years, the wide use of consumer electronic devices has driven the rapid development of lithium ion batteries (LIBs) toward high density, lightweight, long cycle life, and improved safety.[1,2] When compared with the commercial anode material of graphite which has the theoretical capacity of about 372 mA h g^{-1}, transition metal oxides are considered as promising alternatives due to their higher theoretical capacities[3,4] and other superior physical properties.[3,5] However, because of the relatively large polarization at high charge/discharge rates, the induced increase of electrolyte resistance, as well as the drastic volume variation during the Li^+ ion insertion and extraction, these oxide materials typically suffer from the poor cycling stability, which greatly restricts their practical uses as high-performance lithium-ion battery anodes.[5−7] In order to alleviate these problems, preparing novel nanostructured electrode materials has been proved as an efficient way for the better accommodation of strain resulting from lithium insertion/deinsertion, the higher electrode/electrolyte contact area, and the shorter path lengths for both electrons and Li^+ diffusion than the ones of bulk materials.[8,9]

Among various transition metal oxides, Co_3O_4, a mixed valence compound, has attracted tremendous attention owing to its unique physical and chemical properties. Co_3O_4 nanobelts,[10] porous nanocapsules,[11] hexagonal nanoplatelets,[12] nanopolyhedras,[13] and other nanostructures with novel morphologies[14−16] were synthesized and employed as LIB anode materials. Ma and his colleagues successfully synthesized multishelled Co_3O_4 hollow microspheres, which exhibited an excellent capacity of 1615.8 mA h g^{-1}.[17] Porous rhombus-shaped Co_3O_4 nanorods were as well prepared by Mei and co-workers,[18] delivering a capacity of over 1000 mA h g^{-1} at the current density of 1 C. However, the practical application of these materials is still limited to their synthesis methodologies in terms of the complex fabrication process and the slow throughput involved. Despite the continuous progress that has been made recently, developing a facile and reliable method to synthesize high electrochemical performance Co_3O_4 anode materials with large-scale production is highly desirable and remains challenging.

At the same time, two-dimensional nanomaterials with porosity structure are of great interest in LIBs as a result of their high surface−volume ratio, shortened diffusion pathway, abundant Li-insertion channels, and high mechanical property, hence, endowing the long-term cycling stability.[19,20] Furthermore, the control of exposed crystal facets is also crucial for Li-ion storage in order to manipulate the active electrochemical interface. For cobalt oxide nanosheets, Hu et al. first reported

Received: May 18, 2017
Revised: July 18, 2017
Published: August 8, 2017

DOI: 10.1021/acs.jpcc.7b04799
J. Phys. Chem. C 2017, 121, 19002−19009

that unusually high index {112} planes are more reactive than the low index {001} and {011} planes for methane combustion.[21] In the same manner, Xiao et al. demonstrated the octahedral Co_3O_4 with exposed {111} facets being more beneficial to Li cation transport than that of cubic ones with {001} facets.[22] With the above considerations in mind, Lou's group successfully synthesized nearly 100% exposed (001) facets TiO_2 for high reversible lithium ion electrodes at a current density as high as 10 C.[23] Herein, we reported a facile and effective solvothermal method followed by the thermal treatment to synthesize ultrathin Co_3O_4 nanosheets with in-plane pores of which selectively exposed {112} facets as the main external surfaces. When fabricated as LIB anodes, these virtues bestowed the anode materials with an excellent electrochemical performance. Even after 400 cycles at a high current density of 1 A g^{-1}, the capacities could still retain 1090 mA h g^{-1} with the Coulombic efficiency of above 99.5%. All of these would give further insights into the development of high-performance LIB anode materials.

2. EXPERIMENTAL SECTION

2.1. Synthesis of Co_3O_4 Nanomaterials. All chemicals were purchased in the analytical grade and were used without any further purification. In a typical preparation, 3.52 g of $Co(NO_3)_2{\cdot}6H_2O$ was dissolved in 40 mL of methanol. After $Co(NO_3)_2{\cdot}6H_2O$ dissolved completely, 5.9 mL of benzyl alcohol was added to the mixture. After stirring for another 1 h, the solution was transferred into a 100 mL Teflon-lined stainless steel autoclave, which was subsequently heated to 180 °C and maintained for 24 h. Then, it was cooled to room temperature naturally. The resulting precipitate was collected, washed with anhydrous ethanol and deionized water three times respectively, and dried at 60 °C overnight. A lilac powder was obtained and subsequently calcined in air with a ramp rate of 5 °C/min to 400 °C with a duration of 4 h.

2.2. Characterization. The purity and crystalline structure of the samples were characterized by powder X-ray diffraction (XRD) employing a scanning rate of 0.05°/s in a 2θ range from 10° to 80°, using a Bruker D8 Advance (Bruker, Billerica, MA, U.S.A.) instrument equipped with monochromatized Cu Kα radiation. The morphologies and sizes of the samples were observed by SU-8010 field-emission SEM (Hitachi, Tokyo, Japan) at an accelerating voltage of 1.5 kV. Transmission electron microscopy (TEM) and high resolution transmission electron microscopy (HRTEM) were conducted by a Tecnai G20 (FEI, Hillsboro, OR, U.S.A.) using an accelerating voltage of 200 kV. The Brunauer–Emmett–Teller (BET) specific surface areas of the samples were evaluated on the basis of nitrogen adsorption isotherms using a Micromeritics ASAP 2020 gas adsorption apparatus (Micromeritics, Norcross, GA, U.S.A.). X-ray photoelectron spectroscopy (XPS) was recorded on a VG Multilab 2000 (Thermo Fisher Scientific, Waltham, MA, U.S.A.) photoelectron spectrometer using monochromatic Al Kα radiation under vacuum at a pressure of 2×10^{-6} Pa. All of the binding energies were referenced to the C 1s peak at 284.6 eV of the surface adventitious carbon. The infrared spectra were collected using a PerkinElmer Spotlight 400 (PerkinElmer, Waltham, MA, U.S.A.) spectrometer. Spectra were recorded between 400 and 4000 cm^{-1}.

2.3. Electrochemical Measurement. Electrochemical performances of the samples were evaluated in Li test cells. The working electrodes were comprised of the active material, acetylene black, and polytetrafluoroethylene (PTFE) at the weight ratio of 7:2:1. The weight of active material is 0.70 mg. Lithium metal was used as the counter and reference electrodes. The electrolyte was 1 mol L^{-1} $LiPF_6$ dissolved in a 1:1:1 mixture of ethylene carbonate (EC), ethylene methyl carbonate (EMC), and dimethyl carbonate (DMC). The cells were assembled in a glovebox filled with high-purity argon (H_2O and O_2 < 1 ppm). Discharge/charge measurements of the cells were performed between the potential range of 0.01–3.00 V (vs Li^+/Li) using a LAND-CT2001A instrument (LANHE, Wuhan, China). Cyclic voltammograms (CVs) were conducted on a Zahner-Elektrik IM6e electrochemical workstation (Zahner-Elektrik, Kronach, Germany). The CV curves for the above test cells were recorded in a potential range of 0.01–3.00 V (vs Li^+/Li) at a scan rate of 0.05 mV s^{-1} at 25 °C.

3. RESULTS AND DISCUSSION

Figure 1 shows the XRD patterns of the as-prepared precursor and porous Co_3O_4 nanosheets. The high intensity of the peaks

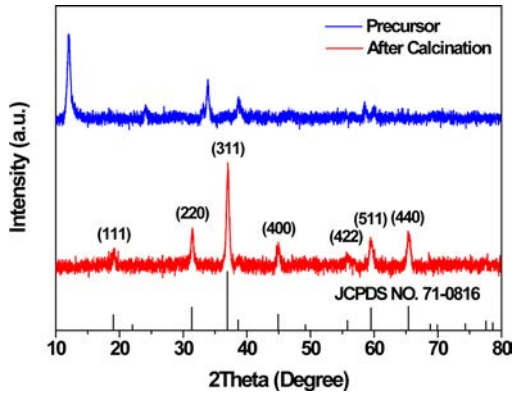

Figure 1. XRD patterns of the precursor and as-synthesized Co_3O_4 nanosheets with the in-plane pores.

at 2θ = 11.8° and 33.8° in the upper pattern (blue) indicates that the as-synthesized precursor is highly crystalline. After calcination at 400 °C for 4 h, 0.8124 g of final product was obtained with an impressively high yield of 83.5% (Figure S1). Also, the bottom pattern (red) displays all of the diffraction peaks of the nanosheet sample being identified as the standard Joint Committee on Powder Diffraction Standards (JCPDS) card no. 71-0816. It is evident that there is not any impurity peaks detected for other phases, indicating the obtained Co_3O_4 being well-crystalline with the cubic structure (space group: $F\bar{4}3m$).

Moreover, the size and morphologies of the precursor and Co_3O_4 nanosheets were studied by SEM, TEM, and HRTEM. The SEM and TEM images in Figure S2 illustrate the precursors composed of hierarchical flower-like microspheres with a diameter of several micrometers, which was assembled by a large number of nanosheets. The obvious dark-light contrast of the nanosheets in TEM images designates their ultrathin texture. After calcination, their morphologies which can be seen from Figure 2 remained mostly the same, except for the formation of a large amount of pores across the nanosheets which could be attributed to the thermal decomposition of metal–organic complexes. The cross-sectional images supported the ultrathin feature with the nanosheet thickness of about 10 nm. As shown in the EDS spectrum in Figure S3, the existence of Co and O elements is observed for the final calcined products. More interestingly, Figures 2d and 3a,b

DOI: 10.1021/acs.jpcc.7b04799
J. Phys. Chem. C 2017, 121, 19002–19009

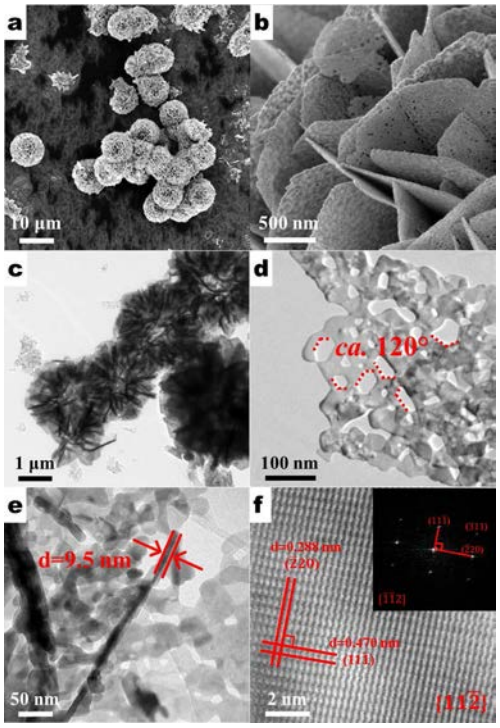

Figure 2. Typical SEM, TEM, and HRTEM images of prepared Co_3O_4 nanosheets with the in-plane pores. (a,b) Different magnification SEM images, (c) low magnification TEM image, (d) vertical view, (e) cross−sectional view, and (f) high resolution TEM image; the inset of panel f gives the corresponding FFT pattern.

illustrate the two adjacent edges of most holes sharing an angle of 120°, in which analogous phenomenona have been reported previously in the literature.[24,25] Specifically, during the growth process, benzyl alcohol is believed to play a critical role as a structure-directing agent, initiating the formation of defects and sheetlike structures.[26,27] After calcination, the precursor decomposed and transformed into Co_3O_4 nanosheets, while the high reaction/etching rate at the defects in Co_3O_4 precursor nanosheets would lead to the construction of those pores/holes.

To better understand the thermal decomposition process, FT-IR was conducted before and after the calcination. Figure 4 dmosnstrates the FT-IR profiles of the uncalcined precursor and the calcined one. The peaks at around 3480, 2870, 1640, and 1070 cm^{-1} are associated with O−H stretching vibrational bands, C−H stretching vibrational bands, and O−C and C═O vibrational bands, respectively. After calcination, there are only

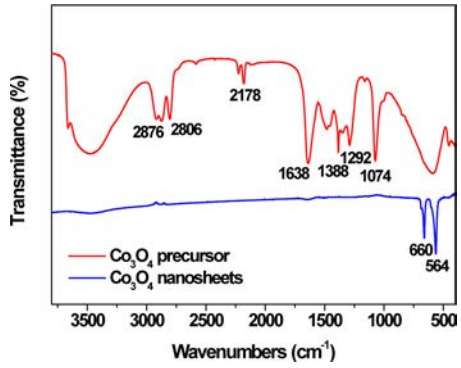

Figure 4. FT-IR spectra the precursor and as-synthesized Co_3O_4 nanosheets.

two distinct absorption bands at 564 and 660 cm^{-1} observed, which are originated from the stretching vibrations of the Co−O bonds, suggesting the organic capping agents being completely removed after the thermal treatment.[28,29]

In addition, visible light-dark contrast and misorientations across the "bridge" of two holes (Figure 3a,b) illustrate the existence of grain boundaries, which can be further confirmed by the ring-shaped pattern in electron diffraction in Figure 3c. The corresponding HRTEM image taken on the flat-surface of the Co_3O_4 porous nanosheets is displayed in Figure 2f, which indicates the high crystallinity with a clearly resolved lattice fringes with *d* values of 0.288 and 0.470 nm, matching up to the value of $(\bar{2}20)$ and $(11\bar{1})$ planes of the Co_3O_4 cubic phase, respectively. Notably, the angle of 90° between these two lattices is also consistent with the theoretical values. Given the above results, we can deduce that these cubic Co_3O_4 nanosheets dominantly exposed high-index $\{11\bar{2}\}$ facets as the external surfaces.

Generally, ultrathin nanostructures are accompanied by the large surface area. To shed light on the surface area of the as-prepared samples, they were characterized by nitrogen adsorption and desorption isotherms at 77.2 K. As depicted in Figure 5, the adsorption−desorption curves exhibit the type-IV isotherm with an H3 hysteresis loop, indicating that the sample shows mesoporous nanostructures and is composed of loose assemblages of sheet-like particles forming slit-like pores.[30,31] The Brunauer−Emmett−Teller (BET) analysis further gives a high specific surface area of 80.35 $m^2\ g^{-1}$ with the pore size distribution peaked at 24.4 and 36.4 nm (upper inset, Figure 5), which is in a agreement with the electron microscopy analysis discussed above.

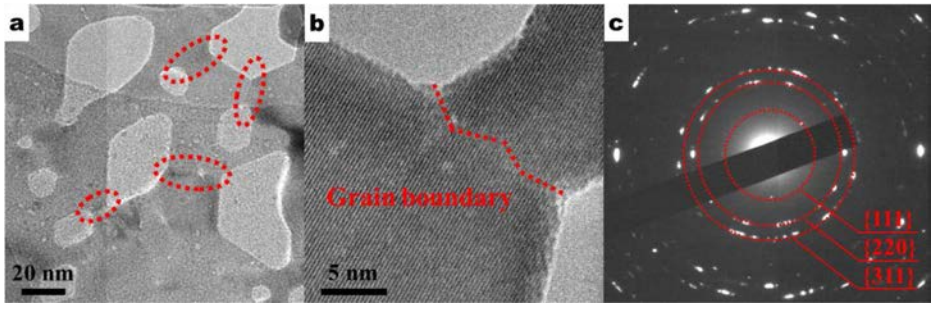

Figure 3. (a,b) High magnification TEM images of selected Co_3O_4 nanosheets with in-plane pores, grain boundaries are marked by red dashed oval in panel a and dashed lines in panel b; (c) corresponding SAED pattern of panel a.

DOI: 10.1021/acs.jpcc.7b04799
J. Phys. Chem. C 2017, 121, 19002−19009

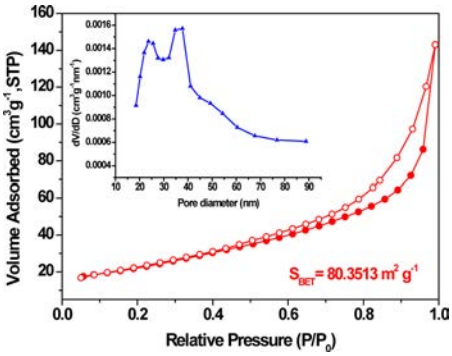

Figure 5. Nitrogen adsorption and desorption isotherm obtained at 77.2 K with the corresponding pore size distribution (inset).

XPS characterizations provide further details into the elemental compositions and chemical states of the exposed surface. There are two characteristic peaks observed at 780.0 and 795.1 eV as displayed in Figure 6a, which can be attributed to the $2p_{3/2}$ and $2p_{1/2}$ orbitals for Co in Co_3O_4, respectively, with a spin−orbit splitting of 15.1 eV.[10] The two satellite peaks located at 786 and 803 eV could be accredited to the generation of oxygen vacancies on the surface.[32,33] The fine-scanned O 1s XPS spectrum is as well shown in Figure 6b, in which the most intense peak centered at 529.65 eV can be assigned to the lattice O in Co_3O_4 phase.[34] The peak located at 530.98 eV results from the formation of surface oxygen defects due to the high etching rate during the calcination process,[32] while the lowest intensity peak positioned at 532.1 eV represents the chemisorbed or dissociated oxygen or OH species on the surface of Co_3O_4.[35] In this case, the large surface area together with the ultrathin structure of nanosheets with the in-plane pores can significantly enlarge the interfaical interaction between electrolytes and anode materials and meanwhile shorten the diffusion pathways of Li cations. The porous feature could also provide the buffer zone and prevent the anode pulverization and structural collapse during the Li^+ ion insertion and extraction processes. At the same time, surface defects generated by the heat treatment can also act as nucleation sites, promoting phase transitions between the redox and charge/mass transfer processes.[36,37] Besides, a higher density of dangling bonds provided by external Co^{2+} and Co^{3+} on the exposed {112} facets not only can provide more active sites for lithium storage but also create negatively charge zones and then drive the Li cations to cluster at the high alloying concentration,[38] further facilitating the lithium ions intercalation−deintercalation process in turn. Enlightened by the aforementioned virtues, we believe that the porous Co_3O_4 ultrathin nanosheets have a promising potential for being an alternative anode materials for Li-ion batteries with the enhanced electrochemical performance.

In order to clarify the energy storage redox mechanism of the Co_3O_4 nanosheets, the cyclic voltammetry (CV) was performed as shown in Figure 7a. In the first cycle of CV curves, an irreversible reduction peak is observed at 0.63 V, which corresponds to the initial reduction of Co_3O_4 to metallic Co and the formation of amorphous Li_2O and a solid electrolyte interphase (SEI) layer.[39] During the subsequent anodic scan, there is a broader peak located at around 2.19 V, which can be ascribed to the reversible oxidation of Co^0 to Co^{2+}/Co^{3+}. From the second cycle, the main reduction peak was positively shifted due to the polarization of the electrode in the first cycle[40] and might be the result of the changes in the Co_3O_4 phase structure and the interfacial property.[41] The subsequent CV curves exhibit good reproducibility and similar shapes, suggesting the high reversibility of lithium storage. The conversion reaction associated with these processes can be described as

$$Co_3O_4 + 8Li^+ + 8e^- \leftrightarrow 4Li_2O + 3Co$$

In addition, Figure 7b demonstrates the 1st, 10th, and 20th charge−discharge curves of anodes made from the Co_3O_4 porous nanosheets. It is clear that there are two distinct voltage plateaus at around 1.20 and 1.09 V in the first discharge curve, which are typically attributed to the reduction processes of Co_3O_4 to CoO (i.e., insertion step) and CoO to metallic Co (i.e., conversion step), respectively.[42,43] The subsequently long and flat voltage plateau further indicates a more stable cycling performance of the porous Co_3O_4 nanosheets. The first discharge could reach as high as 1717 mA h g^{-1}, which is 2-fold higher than that of the theoretical value (890 mA h g^{-1}). However, it illustrated an initial capacity decay down to 1160 mA h g^{-1}, which can be mainly due to the possible irreversible processes, such as the electrolyte decomposition and the inevitable formation of a SEI layer.[39,44] During the 10th and 20th cycles, only one sloping potential range can be observed, and the voltage plateaus appear slightly higher and stay stable during the redox processes. More importantly, as the charge−discharge progressed, a reversible capacity of about 1465 mA h g^{-1} in the 10th cycle gradually increases to about 1708 mA h g^{-1} in the 20th cycle, whereas the longer voltage plateau in the 20th cycle suggests an enhancement of the anode reversibility.

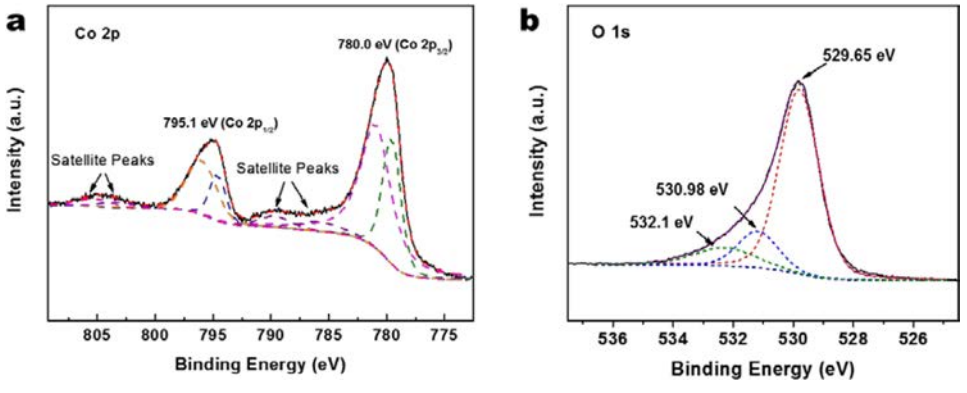

Figure 6. (a) Co 2p and (b) O 1s XPS spectra of porous Co_3O_4 nanosheets.

DOI: 10.1021/acs.jpcc.7b04799
J. Phys. Chem. C 2017, 121, 19002−19009

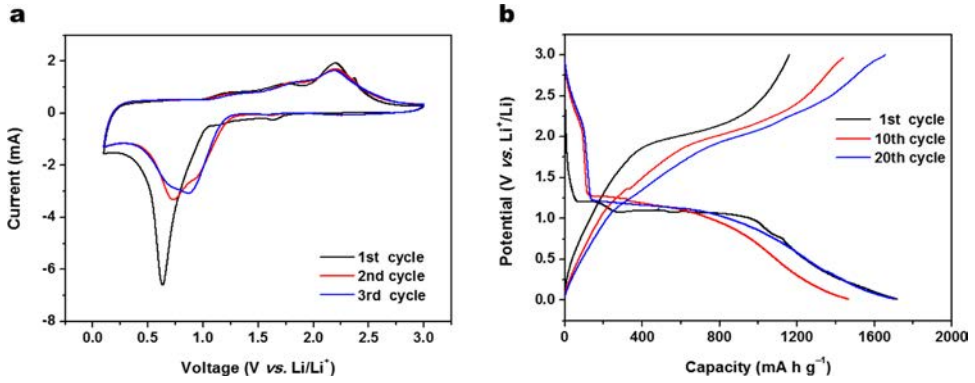

Figure 7. (a) Cyclic voltammetric (CV) curves of the first three cycles at a scan rate of 1 mV s^{-1} between 0.01 and 3.0 V. (b) The 1st, 10th, and 20th charge and discharge curves of Co_3O_4 nanosheets at a current density of 200 mA g^{-1}.

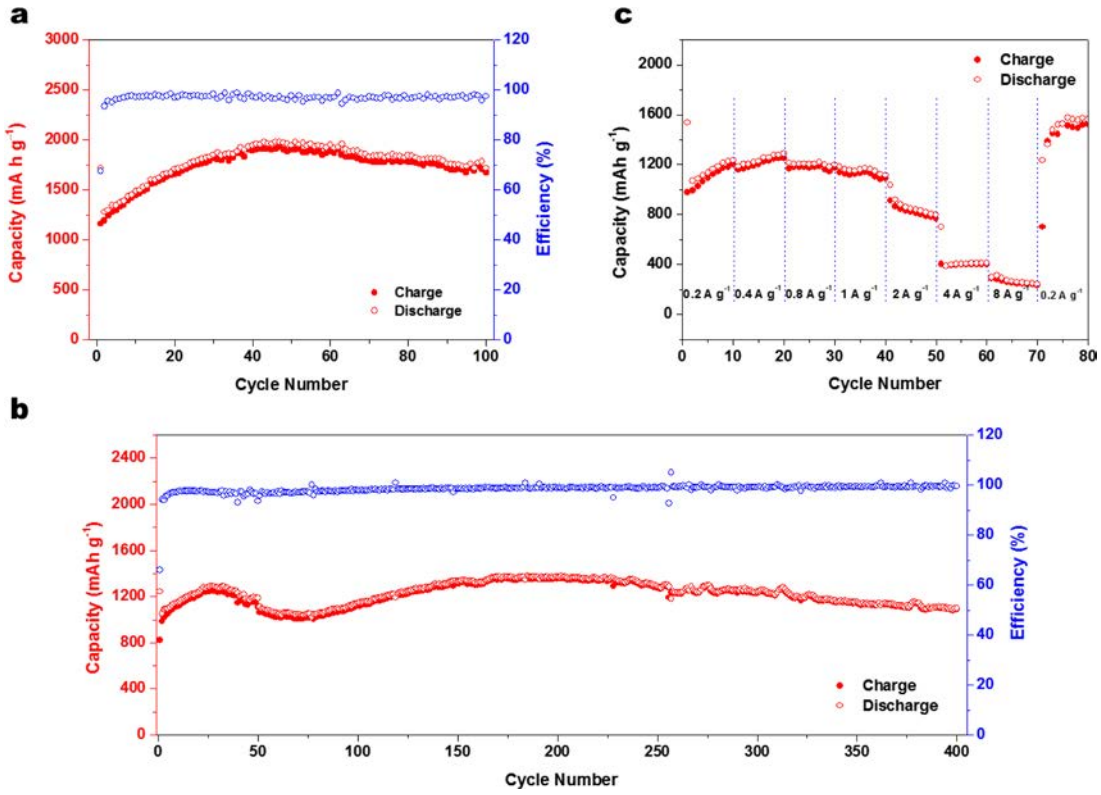

Figure 8. Specific capacity (left) and Coulombic efficiency (right) versus cycle number at current densities of (a) 200 mA g^{-1}; (b) 1 A g^{-1} for Co_3O_4 nanosheets and (c) the rate capacities at different current densities from 0.2 to 8 A g^{-1}.

For the full realization of inherent reversible capacity and percolation of the electrolyte through all of the nanosheets of the electrode, more charge−discharge cycles would be required. The capacity versus cycle number plots at different current densities are then shown in Figure 8. After charging/discharging at a current density of 200 mA g^{-1} for 100 cycles, the retention capacity could be maintained at 1717.2 mA h g^{-1} with a Coulombic efficiency of 97.5% (Figure 8a). There is a gradual increase in the first several decades of cycles and then a decrease subsequently after the capacity reaches 1980 mA h g^{-1}. The capacity fluctuation could be ascribed to the reversible formation of a gel-like layer or the activation-stabilization process of Li-ion diffusion path as proposed in previous reports.[45] The extra capacity obsevered in the cycling test is a common phenomenon when transition metal oxides are applied as anode materials. Most of this extra capacity could be attributed to the reversible formation/dissolution of a polymeric gel-type layer.[46] Moreover, a high density of dangling bonds and grain boundaries on the {112} facet exposed surface could provide more active sites for Li^+ insertion.[47] To further confirm the contribution of {112} facets in this work, similar {112} facet-exposed Co_3O_4 nanosheets with in-plane pores have been prepared just adding urea as precipitant during the hydrothermal reaction, and the specific capacity is higher than theoretical one as well which reaches 930 mA h g^{-1} after 100 cycles at a current density of 200 mA g^{-1} (Figure S4−S6). The ultrathin Co_3O_4 porous nanosheets electrode also exhibits superior rate capability conducted at stepwise rates from 0.2 to 8 A g^{-1} as illustrated in Figure 8b, Remarkably, when the conducted current density decreases from 8 to 0.2 A g^{-1}, a stable high capacity can be maintained at 1670 mA h g^{-1} and displays an uptrend as well. Further investigation in terms of

DOI: 10.1021/acs.jpcc.7b04799
J. Phys. Chem. C 2017, 121, 19002−19009

anode capacity and reversibility was proceeded when increasing the current density to 1 A g^{-1}, and the Co_3O_4 anode can still deliver a capacity of 1090 mA h g^{-1} and Coulombic efficiency up to 99.5% even after a long cycle life of 400 times as depicted in Figure 8c. In contrast with the result at a current density of 200 mA g^{-1}, when prolonged the cycle life, there exists another uphill after the first fluctuation around the 75th cycle, and the capacity increases to 1350 mA h g^{-1} at the 200th cycle and then decreases gradually with an average Coulombic efficiency of 99.1%. Similar results were presented before;[45,48,49] however, the mechanism is still unclear, and no convincing interpretations were given with more thorough research clearly needed. In any case, the ultrathin Co_3O_4 with in-plane pores anode materials shows an excellent electrochemical performance for lithium storage which is a result of combined effects of the following four factors, as shown in Figure 9: (1) the ultrathin

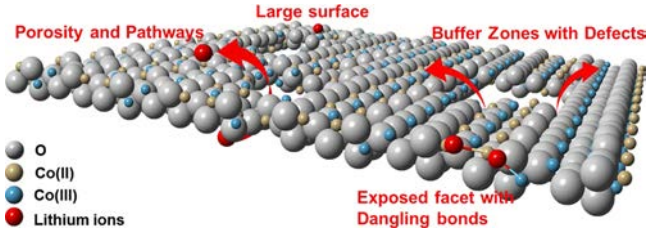

Figure 9. Schematic illustration of different mechanisms contributing to the excellet electrochemical performance of ultrathin Co_3O_4 porous nanosheets for high-performanc Li-ion battery anodes.

structure with the large surface area can shorten diffusion paths and provide substantial electrochemical reaction interface and active sites for lithium ion transport; (2) the porous structure can offer more pathways for lithium ion diffusion and act as a buffer zone for reducing the volume change during lithium ion insertion/extraction processes; (3) the exposed high-index {112} facets with high density of dangling bonds can provide more avctive sites for Li^+ insertion and drive the Li cations to cluster; (4) the oxygen defects on the surface can serve as nucleation sites to promote the phase transition during the electro-redox process. When compared to the recent literature, our Co_3O_4 porous nanosheet materials constitute one of the best-performed Co-based anode materials to date (Table S1). All of these results clearly indicate the excellent capacity and high stable charge−discharge reversibility of the as-prepared nanosheets.

4. CONCLUSIONS

In summary, hierarchical nanostructured Co_3O_4 composed of ultrathin porous nanosheets has been successfully prepared with a high yield of 83.5%. The assembled nanosheets with the thickness of ca. 10 nm predominately expose the active {112} facets. When fabricated as anode materials, these novel Co_3O_4 nanostructures could deliver ultrahigh capacities of 1717 and 1090 mA h g^{-1} at current densities of 200 and 1000 mA g^{-1}, respectively, for a long cycle life. Such excellent anode performance could be attributed to its unique morphology, which could shorten the diffusion of Li^+ ions, buffer the volume expansion, and provide more active sites. It is believed that the facile synthetic method could be further extended to other transition metal oxides or derivates for the alternative high-performance Li-ion battery anodes.

■ ASSOCIATED CONTENT

Supporting Information

The Supporting Information is available free of charge on the ACS Publications website at DOI: 10.1021/acs.jpcc.7b04799.

Production yield and EDS spectrum of the sample; SEM and TEM images of the precursor; TEM, nitrogen adsorption, desorption isotherm, and cyclying results of the comparison sample; and a table comparing the current work with other literature reports. (PDF)

■ AUTHOR INFORMATION

Corresponding Authors

*E-mail: jchu@mail.scuec.edu.cn.
*E-mail: johnnyho@cityu.edu.hk.

ORCID

Renjie Wei: 0000-0002-0459-7196
Tengfei Zhou: 0000-0002-7364-0434
Johnny C. Ho: 0000-0003-3000-8794

Notes

The authors declare no competing financial interest.

■ ACKNOWLEDGMENTS

This work is financially supported by the National Natural Science Foundation of China (Grants 51672229 and 21673300), the Environment and Conservation Fund of Hong Kong SAR, China (ECF 2016-85), the General Research Fund (CityU 11213115) and the Theme-based Research Scheme (T42-103/16-N) of the Research Grants Council of Hong Kong SAR, China, and the Science Technology and Innovation Committee of Shenzhen Municipality (Grant JCYJ20160229165240684), and a grant from the Shenzhen Research Institute, City University of Hong Kong.

■ REFERENCES

(1) Goodenough, J. B.; Park, K. S. The Li-Ion Rechargeable Battery: A Perspective. *J. Am. Chem. Soc.* **2013**, *135*, 1167−1176.
(2) Yang, Z.; Zhang, J.; Kintner-Meyer, M. C. W.; Lu, X.; Choi, D.; Lemmon, J. P.; Liu, J. Electrochemical Energy Storage for Green Grid. *Chem. Rev.* **2011**, *111*, 3577−3613.
(3) Wu, H. B.; Chen, J. S.; Hng, H. H.; Lou, X. W. D. Nanostructured Metal Oxide-Based Materials as Advanced Anodes for Lithium-Ion Batteries. *Nanoscale* **2012**, *4*, 2526−2542.
(4) Reddy, M. V.; Subba Rao, G. V.; Chowdari, B. V. R. Metal Oxides and Oxysalts as Anode Materials for Li Ion Batteries. *Chem. Rev.* **2013**, *113*, 5364−5457.
(5) Poizot, P.; Laruelle, S.; Grugeon, S.; Dupont, L.; Tarascon, J. M. Nano-Sized Transition-Metal Oxides as Negative-Electrode Materials for Lithium-Ion Batteries. *Nature* **2000**, *407*, 496−499.
(6) Lou, X. W.; Deng, D.; Lee, J. Y.; Feng, J.; Archer, L. A. Self-Supported Formation of Needlelike Co_3O_4 Nanotubes and Their Application as Lithium-Ion Battery Electrodes. *Adv. Mater.* **2008**, *20*, 258−262.
(7) Xu, X.; Cao, R.; Jeong, S.; Cho, J. Spindle-like Mesoporous α-Fe_2O_3 Anode Material Prepared from MOF Template for High-Rate Lithium Batteries. *Nano Lett.* **2012**, *12*, 4988−4991.
(8) Aricò, A. S.; Bruce, P.; Scrosati, B.; Tarascon, J.; van Schalkwijk, W. Nanostructured Materials for Advanced Energy Conversion and Storage Devices. *Nat. Mater.* **2005**, *4*, 366−377.
(9) Bruce, P. G.; Scrosati, B.; Tarascon, J.-M. Nanomaterials for Rechargeable Lithium Batteries. *Angew. Chem., Int. Ed.* **2008**, *47*, 2930−2946.
(10) Huang, H.; Zhu, W.; Tao, X.; Xia, Y.; Yu, Z.; Fang, J.; Gan, Y.; Zhang, W. Nanocrystal-Constructed Mesoporous Single-Crystalline Co_3O_4 Nanobelts with Superior Rate Capability for Advanced

DOI: 10.1021/acs.jpcc.7b04799
J. Phys. Chem. C 2017, 121, 19002−19009

Lithium-Ion Batteries. *ACS Appl. Mater. Interfaces* **2012**, *4*, 5974−5980.
(11) Liu, J.; Xia, H.; Lu, L.; Xue, D. Anisotropic Co_3O_4 Porous Nanocapsules toward High-Capacity Li-Ion Batteries. *J. Mater. Chem.* **2010**, *20*, 1506.
(12) Su, D.; Xie, X.; Munroe, P.; Dou, S.; Wang, G. Mesoporous Hexagonal Co_3O_4 for High Performance Lithium Ion Batteries. *Sci. Rep.* **2015**, *4*, 6519.
(13) Huang, G.; Zhang, F.; Du, X.; Qin, Y.; Yin, D.; Wang, L. Metal Organic Frameworks Route to in Situ Insertion of Multiwalled Carbon Nanotubes in Co_3O_4 Polyhedra as Anode Materials for Lithium-Ion Batteries. *ACS Nano* **2015**, *9*, 1592−1599.
(14) Chen, S.; Zhao, Y.; Sun, B.; Ao, Z.; Xie, X.; Wei, Y.; Wang, G. Microwave-Assisted Synthesis of Mesoporous Co_3O_4 Nanoflakes for Applications in Lithium Ion Batteries and Oxygen Evolution Reactions. *ACS Appl. Mater. Interfaces* **2015**, *7*, 3306−3313.
(15) Wang, H.; Zhou, T.; Li, D.; Gao, H.; Gao, G.; Du, A.; Liu, H.; Guo, Z. Ultrathin Cobaltosic Oxide Nanosheets as an Effective Sulfur Encapsulation Matrix with Strong Affinity Toward Polysulfides. *ACS Appl. Mater. Interfaces* **2017**, *9*, 4320−4325.
(16) Yang, J.; Zhou, T.; Zhu, R.; Chen, X.; Guo, Z.; Fan, J.; Liu, H. K.; Zhang, W.-X. Highly Ordered Dual Porosity Mesoporous Cobalt Oxide for Sodium-Ion Batteries. *Adv. Mater. Interfaces* **2016**, *3*, 1500464.
(17) Wang, X.; Wu, X. L.; Guo, Y. G.; Zhong, Y.; Cao, X.; Ma, Y.; Yao, J. Synthesis and Lithium Storage Properties of Co_3O_4 Nanosheet-Assembled Multishelled Hollow Spheres. *Adv. Funct. Mater.* **2010**, *20*, 1680−1686.
(18) Mei, W.; Huang, J.; Zhu, L.; Ye, Z.; Mai, Y.; Tu, J. Synthesis of Porous Rhombus-Shaped Co_3O_4 Nanorod Arrays Grown Directly on a Nickel Substrate with High Electrochemical Performance. *J. Mater. Chem.* **2012**, *22*, 9315−9321.
(19) Zhou, X.; Zhong, Y.; Yang, M.; Zhang, Q.; Wei, J.; Zhou, Z. $Co_2(OH)_2CO_3$ Nanosheets and CoO Nanonets with Tailored Pore Sizes as Anodes for Lithium Ion Batteries. *ACS Appl. Mater. Interfaces* **2015**, *7*, 12022−12029.
(20) Chen, Y.; Pang, W. K.; Bai, H.; Zhou, T.; Liu, Y.-N.; Li, S.; Guo, Z. Enhanced Structural Stability of Nickel−Cobalt Hydroxide via Intrinsic Pillar Effect of Metaborate for High-Power and Long-Life Supercapacitor Electrodes. *Nano Lett.* **2017**, *17*, 429−436.
(21) Hu, L.; Peng, Q.; Li, Y. Selective Synthesis of Co_3O_4 Nanocrystal with Different Shape and Crystal Plane Effect on Catalytic Property for Methane Combustion. *J. Am. Chem. Soc.* **2008**, *130*, 16136−16137.
(22) Xiao, X.; Liu, X.; Zhao, H.; Chen, D.; Liu, F.; Xiang, J.; Hu, Z.; Li, Y. Facile Shape Control of Co_3O_4 and the Effect of the Crystal Plane on Electrochemical Performance. *Adv. Mater.* **2012**, *24*, 5762−5766.
(23) Chen, J. S.; Tan, Y. L.; Li, C. M.; Cheah, Y. L.; Luan, D.; Madhavi, S.; Boey, F. Y. C.; Archer, L. A.; Lou, X. W. Constructing Hierarchical Spheres from Large Ultrathin Anatase TiO_2 Nanosheets with Nearly 100% Exposed (001) Facets for Fast Reversible Lithium Storage. *J. Am. Chem. Soc.* **2010**, *132*, 6124−6130.
(24) Hu, J.; Zhu, K.; Chen, L.; Yang, H.; Li, Z.; Suchopar, A.; Richards, R. Preparation and Surface Activity of Single-Crystalline NiO(111) Nanosheets with Hexagonal Holes: A Semiconductor Nanospanner. *Adv. Mater.* **2008**, *20*, 267−271.
(25) Chen, L.; Hu, J.; Richards, R.; Prikhodko, S.; Kodambaka, S. Synthesis and Surface Activity of Single-Crystalline Co_3O_4 (111) Holey Nanosheets. *Nanoscale* **2010**, *2*, 1657−1660.
(26) Niederberger, M.; Bartl, M. H.; Stucky, G. D. Benzyl Alcohol and Transition Metal Chlorides as a Versatile Reaction System for the Nonaqueous and Low-Temperature Synthesis of Crystalline Nano-Objects with Controlled Dimensionality. *J. Am. Chem. Soc.* **2002**, *124*, 13642−13643.
(27) Bilecka, I.; Niederberger, M. Microwave Chemistry for Inorganic Nanomaterials Synthesis. *Nanoscale* **2010**, *2*, 1358−1374.
(28) Gao, C.; Meng, Q.; Zhao, K.; Yin, H.; Wang, D.; Guo, J.; Zhao, S.; Chang, L.; He, M.; Li, Q.; Zhao, H.; Huang, X.; Gao, Y.; Tang, Z. Co_3O_4 Hexagonal Platelets with Controllable Facets Enabling Highly Efficient Visible-Light Photocatalytic Reduction of CO_2. *Adv. Mater.* **2016**, *28*, 6485−6490.
(29) Xu, R.; Zeng, H. C. Self-Generation of Tiered Surfactant Superstructures for One-Pot Synthesis of Co_3O_4 Nanocubes and Their Close- and Non-Close-Packed Organizations. *Langmuir* **2004**, *20*, 9780−9790.
(30) Wei, R.; Hu, J.; Zhou, T.; Zhou, X.; Liu, J.; Li, J. Ultrathin SnS_2 Nanosheets with Exposed {001} Facets and Enhanced Photocatalytic Properties. *Acta Mater.* **2014**, *66*, 163−171.
(31) Wei, R.; Zhou, T.; Hu, J.; Li, J. Glutatione Modified Ultrathin SnS_2 Nanosheets with Highly Photocatalytic Activity for Wastewater Treatment. *Mater. Res. Express* **2014**, *1*, 025018.
(32) Xu, L.; Jiang, Q.; Xiao, Z.; Li, X.; Huo, J.; Wang, S.; Dai, L. Plasma-Engraved Co_3O_4 Nanosheets with Oxygen Vacancies and High Surface Area for the Oxygen Evolution Reaction. *Angew. Chem., Int. Ed.* **2016**, *55*, 5277−5281.
(33) Wang, Y.; Zhou, T.; Jiang, K.; Da, P.; Peng, Z.; Tang, J.; Kong, B.; Cai, W.-B.; Yang, Z.; Zheng, G. Reduced Mesoporous Co_3O_4 Nanowires as Efficient Water Oxidation Electrocatalysts and Supercapacitor Electrodes. *Adv. Energy Mater.* **2014**, *4*, 1400696.
(34) Xiong, S.; Yuan, C.; Zhang, X.; Xi, B.; Qian, Y. Controllable Synthesis of Mesoporous Co_3O_4 Nanostructures with Tunable Morphology for Application in Supercapacitors. *Chem. - Eur. J.* **2009**, *15*, 5320−5326.
(35) Hsieh, P. T.; Chen, Y. C.; Kao, K. S.; Wang, C. M. Luminescence Mechanism of ZnO Film Investigated by XPS Measurement. *Appl. Phys. A: Mater. Sci. Process.* **2007**, *90*, 317−321.
(36) Liu, D.; Zhang, Y.; Xiao, P.; Garcia, B. B.; Zhang, Q.; Zhou, X.; Jeong, Y. H.; Cao, G. TiO_2 Nanotube Arrays Annealed in CO Exhibiting High Performance for Lithium Ion Intercalation. *Electrochim. Acta* **2009**, *54*, 6816−6820.
(37) Liu, D.; Liu, Y.; Pan, A.; Nagle, K. P.; Seidler, G. T.; Jeong, Y. H.; Cao, G. Enhanced Lithium-Ion Intercalation Properties of V_2O_5 Xerogel Electrodes with Surface Defects. *J. Phys. Chem. C* **2011**, *115*, 4959−4965.
(38) Wan, W.; Zhang, Q.; Cui, Y.; Wang, E. First Principles Study of Lithium Insertion in Bulk Silicon. *J. Phys.: Condens. Matter* **2010**, *22*, 415501.
(39) Wang, L.; Liu, B.; Ran, S.; Huang, H.; Wang, X.; Liang, B.; Chen, D.; Shen, G. Nanorod-Assembled Co_3O_4 Hexapods with Enhanced Electrochemical Performance for Lithium-Ion Batteries. *J. Mater. Chem.* **2012**, *22*, 23541.
(40) Yang, X.; Fan, K.; Zhu, Y.; Shen, J.; Jiang, X.; Zhao, P.; Li, C. Tailored Graphene-Encapsulated Mesoporous Co_3O_4 Composite Microspheres for High-Performance Lithium Ion Batteries. *J. Mater. Chem.* **2012**, *22*, 17278.
(41) Yao, W.; Yang, J.; Wang, J.; Nuli, Y. Multilayered Cobalt Oxide Platelets for Negative Electrode Material of a Lithium-Ion Battery. *J. Electrochem. Soc.* **2008**, *155*, A903.
(42) Mei, W.; Huang, J.; Zhu, L.; Ye, Z.; Mai, Y.; Tu, J. Synthesis of Porous Rhombus-Shaped Co_3O_4 Nanorod Arrays Grown Directly on a Nickel Substrate with High Electrochemical Performance. *J. Mater. Chem.* **2012**, *22*, 9315.
(43) Li, W. Y.; Xu, L. N.; Chen, J. Co_3O_4 Nanomaterials in Lithium-Ion Batteries and Gas Sensors. *Adv. Funct. Mater.* **2005**, *15*, 851−857.
(44) Goodenough, J. B.; Kim, Y. Challenges for Rechargeable Li Batteries. *Chem. Mater.* **2010**, *22*, 587−603.
(45) Dou, Y.; Xu, J.; Ruan, B.; Liu, Q.; Pan, Y.; Sun, Z.; Dou, S. X. Atomic Layer-by-Layer Co_3O_4/Graphene Composite for High Performance Lithium-Ion Batteries. *Adv. Energy Mater.* **2016**, *6*, 1501835.
(46) Zhou, G.; Wang, D. W.; Li, F.; Zhang, L.; Li, N.; Wu, Z. S.; Wen, L.; Lu, G. Q.; Cheng, H. M. Graphene-Wrapped Fe_3O_4 Anode Material with Improved Reversible Capacity and Cyclic Stability for Lithium Ion Batteries. *Chem. Mater.* **2010**, *22*, 5306−5313.
(47) Tian, L.; Zou, H.; Fu, J.; Yang, X.; Wang, Y.; Guo, H.; Fu, X.; Liang, C.; Wu, M.; Shen, P. K.; Gao, Q. Topotactic Conversion Route to Mesoporous Quasi-Single-Crystalline Co_3O_4 Nanobelts with

DOI: 10.1021/acs.jpcc.7b04799
J. Phys. Chem. C 2017, 121, 19002−19009

Optimizable Electrochemical Performance. *Adv. Funct. Mater.* **2010**, *20*, 617−623.
(48) Hu, L.; Yan, N.; Chen, Q.; Zhang, P.; Zhong, H.; Zheng, X.; Li, Y.; Hu, X. Fabrication Based on the Kirkendall Effect of Co_3O_4 Porous Nanocages with Extraordinarily High Capacity for Lithium Storage. *Chem. - Eur. J.* **2012**, *18*, 8971−8977.
(49) Chen, Y. M.; Yu, L.; Lou, X. W. D. Hierarchical Tubular Structures Composed of Co_3O_4 Hollow Nanoparticles and Carbon Nanotubes for Lithium Storage. *Angew. Chem., Int. Ed.* **2016**, *55*, 5990−5993.

DOI: 10.1021/acs.jpcc.7b04799
J. Phys. Chem. C 2017, 121, 19002−19009